Chemical Science

ROYAL SOCIETY OF CHEMISTRY

EDGE ARTICLE

View Article Online
View Journal | View Issue

Cite this: *Chem. Sci.*, 2025, **16**, 4661

All publication charges for this article have been paid for by the Royal Society of Chemistry

Ethanol-assisted synthesis of titanium-rich TS-1 zeolite: a new hexa-coordinated Ti site for efficient propylene epoxidation†

Dapeng Hao,[ab] Xintong Li,[c] Guangyuan He,[d] Risheng Bai,[a] Yang Bai,[a] Tianjun Zhang,[e] Lisu Bai,[ab] Jialiang Li,[ab] Qiang Zhang,[ab] Donghai Mei,[ad] Zhaochi Feng *[f] and Jihong Yu *[ab]

Received 26th December 2024
Accepted 4th February 2025

DOI: 10.1039/d4sc08720h

rsc.li/chemical-science

TS-1 (**MFI**) zeolites are widely utilized in various green oxidation reactions, such as alkene epoxidation and alcohol oxidation. To elevate their catalytic efficacy, strategies such as increasing Ti content or constructing highly active Ti species within zeolite are commonly employed. Here, we synthesized a titanium-rich TS-1 zeolite (Si/Ti ratio of 25.6) with an unprecedented hexa-coordinated Ti species, demonstrating high activity in propylene epoxidation, achieved by utilizing ethanol as a crystal growth modifier through a two-step crystallization strategy. The introduced ethanol regulated the crystallization pathway from the classical to the non-classical route, and enhanced the incorporation of Ti within the TS-1 framework by balancing the insertion of Ti and the crystal growth. The hexa-coordinated Ti species promoted by using ethanol as a crystal growth modifier was identified as $Ti(OH_2)(OSi)_3(OSiOH)_2$ by means of ultraviolet-resonance Raman spectroscopy, X-ray absorption spectroscopy and theoretical calculations, differing from the conventional $Ti(H_2O)_2(OH)_2(OSi)_2$ in TS-1. The as-prepared TS-1 zeolite was applied in the propylene epoxidation reaction, showing exceptional catalytic activity (H_2O_2 conv. 35.6%), high 1,2-propylene oxide selectivity (93.3%), and excellent stability. This work introduces an ethanol-assisted synthesis strategy that facilitates the incorporation of a new hexa-coordinated Ti species into TS-1 zeolite that is highly active in oxidation reactions.

Introduction

Zeolites, a class of crystalline microporous materials, are characterized by regular and diverse micropore structures, tunable acidities, and exceptional thermal and hydrothermal stabilities. These characteristics, coupled with their unique shape-selective catalysis, have established zeolites as pivotal catalysts in various industrial applications, such as petroleum refining, petrochemical, and fine chemical synthesis.[1–11] Among these applications, TS-1 zeolite, a derivative of silicalite-1 (S-1, **MFI**) where titanium atoms isomorphously substitute a part of skeletal silicon atoms, has been a catalyst in the evolution of green oxidation systems with remarkable catalytic performance and substantial industrial potential, utilizing hydrogen peroxide as the oxidant, thus garnering significant attention since its inception in 1983.[12] It has found extensive use in the selective oxidation of olefins to epoxides, the ammoximation of cyclohexanone, the oxidation of alcohols to aldehydes or ketones, and the hydroxylation of aromatics, among other green oxidation reactions.[13–21]

The particle size, morphology, and porosity of zeolites are recognized as pivotal factors influencing their catalytic activities.[22–24] Furthermore, the strategic control over the distribution and content of active sites within zeolites is essential for enhancing catalytic performance.[25,26] In TS-1 zeolites, the catalytic activities are intricately linked to the amount, location, and state of the active Ti species. The introduction of Ti into the zeolite framework could lead to structural deformation, so the Ti content of TS-1 is usually less than 2 wt%. Increasing the Ti content within the TS-1 framework is

[a]State Key Laboratory of Inorganic Synthesis and Preparative Chemistry, College of Chemistry, Jilin University, 2699 Qianjin Street, Changchun 130012, P. R. China. E-mail: jihong@jlu.edu.cn

[b]International Center of Future Science, Jilin University, 2699 Qianjin Street, Changchun 130012, P. R. China

[c]Shanghai Key Laboratory of Green Chemistry and Chemical Processes, School of Chemistry and Molecular Engineering, East China Normal University, Shanghai 200062, P. R. China

[d]School of Materials Science and Engineering, Tiangong University, Tianjin 300387, P. R. China

[e]State Key Laboratory of New Pharmaceutical Preparations and Excipients, Key Laboratory of Medicinal Chemistry and Molecular Diagnosis of the Ministry of Education, College of Chemistry and Materials Science, Hebei University, 071002, P. R. China

[f]State Key Laboratory of Catalysis, Dalian Institute of Chemical Physics, Chinese Academy of Sciences, 457 Zhongshan Road, Dalian, 116023, P. R. China. E-mail: zcfeng@dicp.ac.cn

† Electronic supplementary information (ESI) available. See DOI: https://doi.org/10.1039/d4sc08720h

a direct approach to boosting their catalytic activities. However, the rate mismatch between the Si and Ti atoms in framework incorporation often leads to the formation of detrimental anatase species during synthesis.[27–29] To circumvent these issues, researchers regulated the TS-1 zeolite crystallization process, employing crystal growth modifiers (CGMs) to increase framework Ti content and mitigate the formation of anatase.[30–32] Tatsumi and coworkers made the TS-1 zeolite crystallization process change from the liquid phase crystallization mechanism to the solid phase crystallization mechanism by adding $(NH_4)_2CO_3$ into the synthesis solution, effectively increasing the Ti content to reduce the Si/Ti ratio of 34.[28] In addition to $(NH_4)_2CO_3$, the addition of glycine, acrylic acid, or 1,3,5-benzene-carboxylic acid (H_3BTC) has shown promise in altering the crystallization mechanism from the liquid-phase transformation mechanism to the solid phase crystallization mechanism, thus enhancing the Ti incorporation.[33–38] However, the addition of CGMs increases the preparation cost of TS-1 zeolite, and the mechanism by which the CGMs affect the crystallization of zeolites remains unclear. These problems have brought challenges to the preparation of TS-1 zeolite with high Ti content by adding CGMs.

Furthermore, the crystallization pathway of zeolites encompassing both classical and nonclassical routes has a significant influence on the formation of titanium species.[28] The fundamental building blocks, such as monomers, oligomers, precursors, and nanoparticles, during the crystallization process play a crucial role in determining the chosen crystallization route. The classical pathway is characterized by spontaneous nucleation, followed by the addition of atoms or molecules to create a smooth crystal surface. In contrast, the non-classical pathway involves the incorporation of oligomers or primary nanoparticles, leading to crystals with irregular surfaces and mesoporous architectures. Yu and co-workers have shown that switching between these crystallization routes in TS-1 zeolites can be manipulated to control the formation of active titanium sites by carefully regulating the crystallization kinetics.[15,17,38] Thus, strategically controlling the crystallization pathway emerges as a promising approach to constructing and modulating the activity of Ti sites. In the realm of propylene epoxidation, the type of Ti species present in TS-1 zeolites significantly impacts catalytic performance. Previous studies have revealed that hexa-coordinated Ti species ("TiO_6") exhibit higher activity than their tetra-coordinated counterparts ("TiO_4") owing to their proximity to Si vacancies within the TS-1 framework.[25] Post-treatment methods have been employed to convert "TiO_4" to more active species, such as penta-coordinated (Ti-V) and hexa-coordinated (Ti-VI), with the latter being identified as highly active for propylene epoxidation.[25] Nevertheless, the Ti–OH group of the hexa-coordinated Ti species, as an acid site, is prone to secondary reactions, forming by-products (2-methoxypropan-1-ol, 1-methoxypropan-2-ol (MMA) and 1,2-propanediol (PG)), resulting in decreased selectivity of the target product 1,2-propylene oxide (PO).[37] Therefore, constructing active hexa-coordinated Ti species that are located near the framework defects and are free of Ti–OH groups could contribute to the development of propylene epoxidation catalysts.[25,39]

Herein, anatase-free TS-1 zeolites with a high Ti content (Si/Ti = 25.6) have been successfully synthesized using ethanol as a crystal growth regulator combined with a two-step crystallization strategy. The incorporation of ethanol changes the crystallization path from the classical to non-classical route and facilitates the incorporation of Ti into TS-1 zeolite frameworks. Ultraviolet resonance Raman (UV Raman) spectroscopy, X-ray absorption spectroscopy (XAS), and density functional theory (DFT) calculations reveal that the hexa-coordinated Ti species in ethanol-assisted TS-1 adopts a structure of $Ti(OH_2)(OSi)_3(\text{-}OSiOH)_2$, which is a new type of Ti species connected at Si–OH and distinct from the conventional "TiO_6" with the structure of $Ti(H_2O)_2(OH)_2(OSi)_2$. Note that the ethanol-assisted TS-1 shows a significant catalytic activity in propylene epoxidation, achieving a H_2O_2 conversion of 35.6%, which is superior to the conventional "TiO_6" with the structure of $Ti(H_2O)_2(OH)_2(OSi)_2$ containing TS-1 (17.4%). This study provides a new strategy by the employment of ethanol as a crystal growth modifier for the synthesis of anatase-free TS-1 zeolites with elevated Ti content, featuring a highly active hexa-coordinated Ti species for propylene epoxidation.

Results and discussion

The Ti-rich anatase-free TS-1 zeolite was hydrothermally synthesized by an ethanol-assisted two-step crystallization (80/170 °C) strategy with a molar composition of $1.0SiO_2$: $0.033TiO_2$: 0.2tetrapropyl ammonium hydroxide (TPAOH) : $9H_2O$: 1.5 CH_3CH_2OH, and the sample was named TS-1-E-80-170. As a comparison, conventional TS-1 zeolite (TS-1-C-80-170) was hydrothermally synthesized by a two-step crystallization strategy with the same method but free of ethanol. To elucidate the mechanism by which ethanol and the two-step crystallization affect the properties of TS-1 zeolite, comprehensive characterization of TS-1-E-80-170, TS-1-C-80-170 (both crystallized at 80 °C for 48 h and then crystallized at 170 °C for 15 h) and TS-1-E-170 (directly crystallized at 170 °C for 63 h) was performed. As shown in Fig. S1,† the X-ray diffraction (XRD) patterns of the three samples exhibit the **MFI** topology, which proves the phase purity of the TS-1 zeolites. The scanning electron microscopy (SEM) images of the TS-1 samples are shown in Fig. S2.† TS-1-C-80-170 shows an oval or spheroidal morphology, whereas TS-1-E-80-170 and TS-1-E-170 exhibit a sheet-like morphology, which indicates that the presence of ethanol affects the morphology of TS-1 zeolites. The transmission electron microscopy (TEM) images show that the crystal size of TS-1-E-80-170 and TS-1-C-80-170 ranges from 50 to 150 nm, whereas for TS-1-E-170, it extends from 200 to 300 nm (Fig. 1a, b and S3–5†). This observation implies that the two-step crystallization process is advantageous in reducing the crystal size, a phenomenon attributed to the preferential nucleation at lower temperatures. The N_2 adsorption/desorption isotherms, as depicted in Fig. S6a,† exhibit a hysteresis loop within the pressure range of $0.9 < P/P_0 < 1.0$, attributed to the interparticle voids from the stacking of small

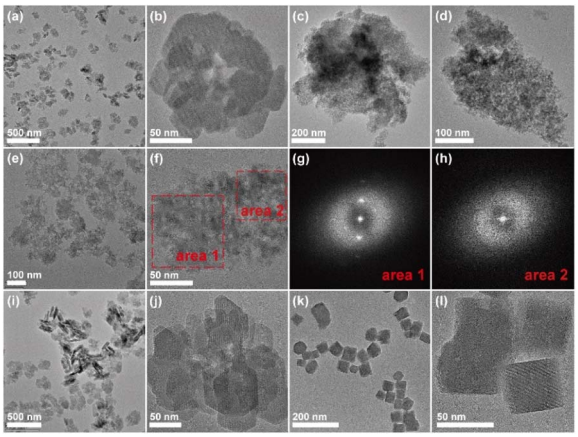

Fig. 1 (a) Low and (b) high magnification TEM images of TS-1-E-80-170. TEM images of TS-1-E-80-170 crystallized at 80 °C for 48 h and then at 170 °C for (c) 3 h and (d) 6 h, (e and f) 10 h, and (i and j) 48 h. (g and h) FFT diffractograms of area 1 and area 2 in (f). (k) Low and (l) high magnification TEM images of TS-1-C-80-170 crystallized at 80 °C for 48 h and then at 170 °C for 48 h.

crystal particles. The Horvath–Kawazoe (H–K) pore size distributions of TS-1-E-80-170, TS-1-C-80-170, and TS-1-E-170 show that the micropores of all three samples are mainly distributed at 0.5–0.6 nm (Fig. S6b†). TS-1-E-80-170, TS-1-C-80-170, and TS-1-E-170 show the same micropore volume of 0.14 $cm^3\ g^{-1}$, revealing that the microporous structures of the three samples are similar (Table S1†). The two-step crystallized samples TS-1-E-80-170 and TS-1-C-80-170 show higher external surface than the one-step crystallized sample TS-1-E-170. This finding supports the conclusion that the two-step crystallization process is conducive to reducing crystal size, as observed in the TEM images.

We also investigated the crystallization processes of the TS-1 samples prepared in the presence or absence of ethanol (Fig. 1c–h, S7 and S8†) by TEM and XRD measurements. As for TS-1-E-80-170, no solid products could be obtained after the low-temperature crystallization process at 80 °C (Fig. S9†), and when extending the crystallization time for the high-temperature crystallization process (170 °C) from 3 h to 6 h, amorphous substances could be obtained (Fig. 1c and d), as evidenced by the XRD patterns (Fig. S7†). At a crystallization time of 10 h, a time-resolved intermediate crystallization stage can be observed (Fig. 1e and f), where the crystalline phase (area 1 and the corresponding fast Fourier transform (FFT) diffractogram in Fig. 1g) is covered with some amorphous particles (area 2, and Fig. 1h), suggesting the presence of a non-classical crystallization process, with the crystal growth behavior featuring the addition of small particles during the crystallization process. Following 15 h of crystallization, the amorphous substances were predominantly absent, yielding TS-1 crystals with sizes of about 150 nm (Fig. 1a and b). It is notable that when extending the crystallization process of TS-1-E-80-170 to 48 h, the crystallinity of the crystal could be further improved (Fig. 1i, j, S7, and Table S2†). TEM images show that these crystals are composed of small aggregated crystals and show a rough crystal surface (Fig. 1i and j), further indicating that the non-classical crystallization route may be the dominant crystallization process. However for the control sample TS-1-C-80-170 crystallized at 170 °C for 48 h in the absence of the ethanol (Fig. 1k, l, and S8†), crystals with smooth surface could be obtained, showing that the classical crystallization process, characterized by the addition of Si and/or Ti monomers, prevails. As such, the crystallization process of TS-1 zeolite could be affected by the introduction of ethanol, which dramatically prolongs the crystallization time and tailors the dominant crystallization pathways, and eventually, might achieve the regulation of the introduced Ti species.

As shown in Fig. S10,† the Ti content, as measured by inductively coupled plasma (ICP) analysis, in the as-synthesized TS-1-E-80-170 was significantly higher than that in the TS-1-C-80-170. This finding indicated that the presence of ethanol facilitated the incorporation of more Ti into the framework. In the TS-1-C-80-170 samples, the Ti content increased as the crystallization time increased, reaching its highest value upon near completion of crystallization. This suggests that during the crystal growth of TS-1-C-80-170, Si species polymerized with each other at a much faster rate than the condensation of Si species and Ti species, which makes the Si/Ti ratio of the TS-1-C-80-170-3h much higher than that of the initial gel (62 *vs.* 30). With the rapid completion of crystallization, Ti species were difficult to insert into the zeolite framework. In contrast, the Si/Ti ratio in the TS-1-E-80-170 samples remained nearly constant (approximately 30) throughout the 170 °C crystallization stage (3–10 hours), similar to that of the initial gel. The dominance of the non-classical crystallization pathway in the crystallization process of the TS-1-E-80-170 samples facilitated the incorporation of Ti during crystallization, thus improving the Ti content of the final product. The ultraviolet–visible diffuse reflectance (UV-vis) spectrum of TS-1-E-80-170 shows peaks at 210 nm, 260 nm, and 330 nm, ascribed to "TiO_4", highly coordinated Ti

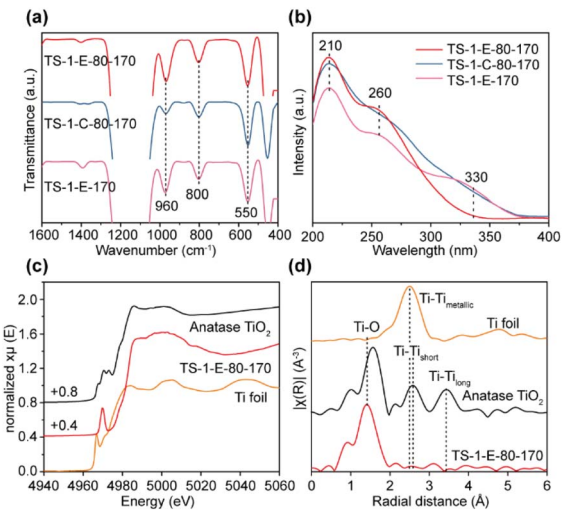

Fig. 2 (a) FT-IR spectra and (b) UV-vis spectra of TS-1-E-80-170, TS-1-C-80-170, and TS-1-E-170. (c) Ti K-edge XANES spectra and (d) Fourier transform k^2-weighted Ti EXAFS spectra in R-spacing of TS-1-E-80-170, anatase, and Ti foil reference.

and anatase, respectively. The absence of the signal at 330 nm suggests the absence of the anatase species (Fig. 2b and S11†).[17,37,40] In contrast, anatase began to form at the early crystallization stage of 3 h of the TS-1-C-80-170 sample (Fig. S12†). This result indicates that the presence of ethanol is beneficial to inhibit the formation of anatase.

Thermogravimetric (TG) analyses (Fig. S13†) show that the weight loss of the TS-1-E-80-170 sample is similar to that of TS-1-C-80-170 (16 *vs.* 18 wt%), and the degradation of the organic species is mostly due to TPA^+. X-ray photoelectron spectroscopy (XPS) analysis reveals that the Si 2p peak of the calcined TS-1-E-80-170 sample shifts to higher binding energy levels (from 103.6 eV to 104.2 eV) compared to those of the uncalcined TS-1-E-80-170 sample (Fig. S14†). Moreover, the peak position of TS-1-C-80-170 exhibits the same shift after calcination (103.4 eV *vs.* 104.0 eV), indicating that the peak position changes can be ascribed to the removal of TPA^+.

ICP analysis gives the Si/Ti ratios for TS-1-E-80-170 (Si/Ti = 25.6), TS-1-C-80-170 (Si/Ti = 50.0), and TS-1-E-170 (Si/Ti = 24.6), indicating that the incorporation of ethanol is observably beneficial to increase the content of Ti in TS-1 zeolites. The O, Si, and Ti species are evenly distributed throughout the TS-1 zeolite as revealed by the elemental distributions of TS-1-E-80-170 (Fig. S15†). Fourier transform infrared spectroscopy (FT-IR) was used to detect the Ti species in the TS-1 zeolite framework (Fig. 2a). The bands that appear at 960 cm^{-1} are attributed to the stretching vibrations of the zeolite framework Si–O–Ti bonds, while the bands at 800 cm^{-1} are characteristic of the **MFI** topology.[37] The intensity ratio between 960 and 800 cm^{-1} ($I_{960/800}$) bands in the FT-IR spectrum is commonly used to assess the relative content of the framework Ti species.[22] As shown in Fig. S16,† TS-1-E-80-170 and TS-1-E-170 show higher $I_{960/800}$ values (1.81 and 1.80, respectively) compared to TS-1-C-80-170 (0.78), indicating a preference for incorporating the Ti species in the TS-1 zeolite framework through the ethanol-assisted method. The existence of framework Ti in TS-1 zeolites was further confirmed by ^{29}Si MAS NMR spectroscopy (Fig. S17†). The presence of acromion at −116 ppm is evidence of Ti species incorporated into the zeolite framework.[28] The spectra of all three samples show the signals at −102 and −113 ppm, attributed to the $Si(OH)(OSi)_3$ (Q^3) and $Si(OSi)_4$ (Q^4) silicon atoms, respectively. Notably, the −113 ppm signal is dominant, which implies that most of the Si atoms have tetrahedral coordination in the form of Q^4. In other words, the structure of the TS-1 zeolites is intact.

UV-vis spectra were employed to detect the Ti species in the TS-1 zeolite. As is shown in Fig. 2b, a strong absorption band at about 210 nm is observed in TS-1-E-80-170, TS-1-C-80-170, and TS-1-E-170 samples. It originates from the electronic transfer between isolated tetrahedrally coordinated titanium and oxygen in the zeolite framework, indicating the existence of isolated framework "TiO_4" species.[40] The Ti species with higher coordination states in TS-1 zeolite are observed in all three samples, as shown by the UV-vis absorption bands at 260 nm.[41] The absorption band positions of TS-1-E-80-170 and TS-1-C-80-170 are different (253 nm *vs.* 260 nm), speculating that the addition of ethanol led to formation of distinct, highly coordinated titanium species in TS-1-E-80-170. It is worth underlining that both TS-1-C-80-170 and TS-1-E-170 show an absorption band at 330 nm, indicating the existence of anatase. There is no absorption band at 330 nm in TS-1-E-80-170, which shows that the combination of the ethanol-assisted method and two-step crystallization is beneficial to the synthesis of TS-1 without the formation of anatase. Anatase is harmful to the H_2O_2-involved oxidation reactions like propylene epoxidation, because it causes easily non-productive decomposition of H_2O_2. The analysis of the Ti species in TS-1 was performed through XPS (Fig. S18†). The peaks at 460.6 eV in all three samples indicate that all the Ti species are tetravalent. The structure of the Ti species in TS-1-E-80-170 was further studied by X-ray absorption spectroscopy (XAS) at the Ti K-edge. The Ti K-edge X-ray absorption near-edge structure (XANES) spectrum in Fig. 2c indicates that the Ti species in TS-1-E-80-170 possess a higher oxidation state than the Ti foil and a closer oxidation state to TiO_2. As shown in Fig. 2d, the extended X-ray absorption fine structure (EXAFS) spectrum of TS-1-E-80-170 shows no obvious Ti–Ti bonds in stark contrast to anatase, while a major peak of the Ti–O bond is detected. This evidence confirms that all titanium atoms are monodispersed within the zeolite framework, and no adjacent pairs of titanium atoms are present. This strongly supports the conclusion that the highly coordinated titanium species in TS-1-E-80-170 are mononuclear in nature.

To further explore the effects of ethanol introduction on Ti species in TS-1, ultraviolet resonance Raman (UV Raman) spectroscopy with excitation wavelengths of 244, 257, 266, and 325 nm was used. The UV Raman spectra of TS-1-E-80-170, TS-1-C-80-170 and TS-1-E-170 samples are shown in Fig. 3. The spectra of the three samples excited at 244 nm (Fig. 3a) show peaks at 380, 490, 530, 800, and 1125 cm^{-1}. The peaks at 380 and 800 cm^{-1} belong to the **MFI** topology in the TS-1 zeolite. The peak at 1125 cm^{-1} is attributed to the Ti–O–Si bond, and

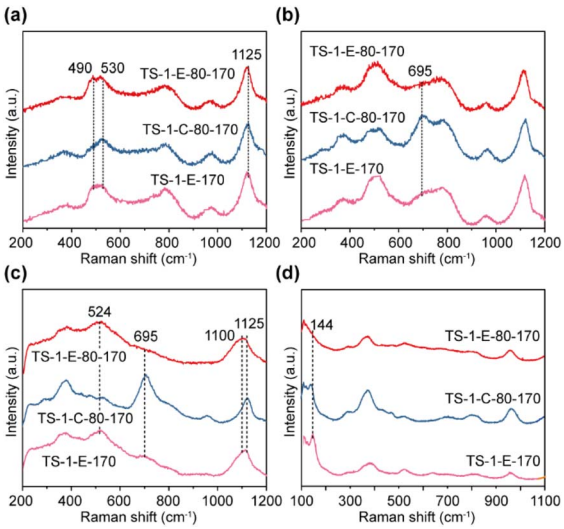

Fig. 3 UV Raman spectra of TS-1-E-80-170, TS-1-C-80-170, and TS-1-E-170 samples excited at (a) 244 nm, (b) 257 nm, (c) 266 nm, and (d) 325 nm.

only when peaks at 490, 530, and 1125 cm^{-1} are present at the same time can it indicate that there is a "TiO_4" in the sample.[25] The above results show that all three samples have tetrahedral "TiO_4", which is consistent with the results of UV-vis spectra. At an excitation wavelength of 257 nm, the UV Raman spectrum of TS-1-C-80-170 exhibits a peak at 695 cm^{-1} (Fig. 3b), and when the excitation wavelength shifted to 266 nm (Fig. 3c), the intensity of the peak increased, indicating the presence of $Ti(H_2O)_2(OH)_2(OSi)_2$ species in TS-1-C-80-170.[28] In contrast, there are no peaks at 695 cm^{-1} observed in the UV Raman spectra of TS-1-E-80-170 and TS-1-E-170 excited at 257 nm and 266 nm, indicating that there are no such $Ti(H_2O)_2(OH)_2(OSi)_2$ species in TS-1-E-80-170 and TS-1-E-170 synthesized by the ethanol-assisted method. It is noteworthy that in the UV Raman spectra of the titanosilicate zeolite samples excited at 266 nm, alongside the peak at 1125 cm^{-1} attributed to the Ti–O–Si stretching vibration,[25] two additional peaks appear at 524 cm^{-1} and 1100 cm^{-1} in the TS-1-E-80-170 and TS-1-E-170 samples, suggesting the possible formation of new hexa-coordinated Ti species. This suggests that the introduction of ethanol in the synthesis could greatly change the type of Ti species in TS-1 zeolite. The UV Raman spectrum excited at 325 nm was used to investigate the anatase species in TS-1 zeolite, with 144 cm^{-1} as the characteristic peak. Fig. 3d shows the absence of anatase in the TS-1-E-80-170 sample, and the presence of anatase in TS-1-C-80-170 and TS-1-E-170 samples. These findings indicate that the ethanol-assisted synthesis combined with the two-step crystallization process effectively suppresses the formation of anatase and facilitates the construction of new hexa-coordinated Ti species.

Combined with the above characterization results of the new type of Ti species in TS-1-E-80-170, DFT calculations were performed to confirm the allocations of Raman peaks and establish the coordination structures of the new Ti species in TS-1-E-80-170. The Raman peaks observed by DFT calculations and experiments are listed in Table S3.† As seen, the calculated Raman peaks are in good agreement with the experimentally observed peaks, confirming the coordination structure of the new Ti species as shown in Fig. 4a. The Raman peaks at 524 and 1100 cm^{-1} are due to the wagging vibration of its Ti–O–Si–OH bonds. Hence, this new type of Ti species is confirmed as a hexa-coordinated Ti species containing three Ti–O–Si bonds, two Ti–O–Si–OH bonds, and one Ti–OH_2 bond, and it can be expressed as having a chemical structure of $Ti(OH_2)(OSi)_3(OSiOH)_2$. Table S4† provides a comprehensive summary of the Raman peaks associated with various titanium (Ti) species, as identified through DFT calculations and experimental observations.[25,41]

The propylene oxide process with H_2O_2 as the oxidant is considered to be the most advantageous process for the production of 1,2-propylene oxide. In the propylene epoxidation reaction, the hexa-coordinated Ti species is more active than the "TiO_4", in which the hexa-coordinated Ti species could form Ti-peroxide transition state intermediates more easily. This is because the hexa-coordinated Ti species is less constrained by the zeolite framework, and its active transition state intermediates have smaller steric hindrance, which can provide an uncrowded catalytic reaction environment.[25,37] Nevertheless, the Ti–OH group of the hexa-coordinated Ti species, as an acid site, is prone to secondary reactions, forming by-products (2-methoxypropan-1-ol, 1-methoxypropan-2-ol, and 1,2-

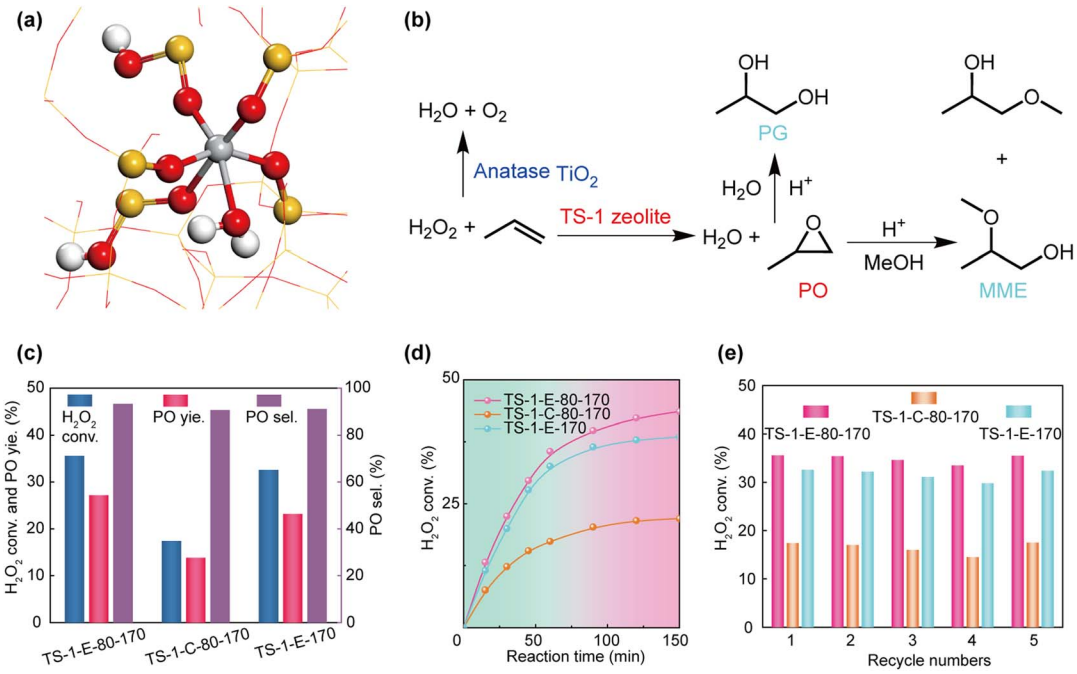

Fig. 4 (a) Proposed structure of the $Ti(OH_2)(OSi)_3(OSiOH)_2$ by DFT. The grey ball represents the Ti atom, while yellow stands for Si, red for O, and white for H. (b) Reaction pathways in the TS-1/MeOH/H_2O_2-catalyzed propylene epoxidation. (c) H_2O_2 conversion, PO yield, and PO selectivity, (d) H_2O_2 conversion at different reaction times and (e) H_2O_2 conversion of the recycle test over different TS-1 zeolites. The samples were calcined at 550 °C for 6 h after four cycle.

propanediol), resulting in reduced selectivity of the main product 1,2-propylene oxide (Fig. 4b). Therefore, the $Ti(OH_2)(-OSi)_3(OSiOH)_2$ species, with no Ti–OH group and only one H_2O coordination, formed by the ethanol assisted synthesis method, have the potential to improve both catalytic activity and selectivity of propylene epoxidation. We evaluated the catalytic properties of TS-1-E-80-170, TS-1-C-80-170, and TS-1-E-170 by the epoxidation of propylene reaction. As shown in Fig. 4c and Table S5,† when the reaction time was 1 h, the $X(H_2O_2)$ and Y(PO) of TS-1-E-80-170 were significantly higher than those of TS-1-C-80-170 (35.6% *vs.* 17.4%, 27.2% *vs.* 13.8%). In Table S6,† we calculated the content of different Ti species, including the tetra- and hexa-coordinated Ti and anatase species, in TS-1-E-80-170, TS-1-C-80-170, and TS-1-E-170 from UV-vis spectra (Fig. S19†), and then calculated the turnover number (TON) of each part, especially the newly constructed hexa-coordinated $Ti(OH_2)(OSi)_3(OSiOH)_2$ and conventional hexa-coordinated $Ti(H_2O)_2(OH)_2(OSi)_2$. The results showed that $Ti(OH_2)(OSi)_3(-OSiOH)_2$ in the TS-1-E-80-170 catalyst exhibited a higher catalytic activity of propylene epoxidation than conventional hexa-coordinated $Ti(H_2O)_2(OH)_2(OSi)_2$ in TS-1-C-80-170 (TON: 546 *vs.* 515). In addition, TS-1-E-80-170 also exhibited a higher S(PO) than TS-1-C-80-170 (93.3% *vs.* 90.6%), ascribed to the absence of Ti–OH groups in $Ti(OH_2)(OSi)_3(OSiOH)_2$, which tend to promote the solvolysis of PO with MeOH and/or H_2O. Fig. 4d shows the change of the conversion of H_2O_2 ($X(H_2O_2)$) of the three samples with the reaction time. The $X(H_2O_2)$ of TS-1-E-80-170 is the highest among the three samples over the catalytic process, suggesting the high catalytic activity of TS-1-E-80-170 in propylene epoxidation reactions. Moreover, the $X(H_2O_2)$ are maintained over the three samples for five cycles with no loss of catalytic activity, which indicates that these samples have high cycling stabilities in propylene epoxidation (Fig. 4e). XRD patterns, UV-vis spectra, TEM, and N_2 adsorption/desorption isotherms show that the crystal structure and the Ti species of TS-1-E-80-170 are well maintained after five cycles, implying high catalytic stability (Fig. S20–23 and Table S1†). We compared the performance of TS-1-E-80-170 with that of reported propylene epoxidation catalysts, as shown in Table S7.† The PO formation rate of TS-1-E-80-170 is among the top level of the reported catalysts, indicating that TS-1-E-80-170 and $Ti(OH_2)(OSi)_3(OSiOH)_2$ species have great potential in the propylene epoxidation reaction.

Conclusions

In summary, anatase-free TS-1 zeolites with elevated Ti content (Si/Ti = 25.6) were successfully synthesized by employing ethanol as an economic crystal growth regulator combined with a two-step crystallization strategy. The addition of ethanol changes the way of nucleation, and consequently changes the crystallization path from the classical route to a non-classical pathway. Moreover, the addition of ethanol to the synthesis gel drastically results in a slow crystallization rate, thus making the speed for the incorporation of Ti into the framework and the crystallization rate match well. Higher Ti content and more condensation time between Ti–OH and Si–OH groups lead to the construction of an unprecedented hexa-coordinated Ti species with the structure of $Ti(OH_2)(OSi)_3(OSiOH)_2$, showing high catalytic performance in the propylene epoxidation reaction (H_2O_2 conversion of 35.6% and PO selectivity of 93.3%) and outstanding stability. This study provides a novel strategy for constructing new Ti active sites and increasing Ti content in TS-1 zeolites by regulating the crystallization kinetics, and may provide new guidance for further optimization of oxidation catalysts.

Data availability

All data associated with this article have been included in the main text and ESI.†

Author contributions

Dapeng Hao: conceptualization, formal analysis, investigation, writing-original draft preparation. Xintong Li: formal analysis, investigation. Guangyuan He: formal analysis, investigation. Risheng Bai: formal analysis, validation. Yang Bai: formal analysis. Tianjun Zhang: formal analysis. Lisu Bai: validation. Jialiang Li: formal analysis. Qiang Zhang: validation. Donghai Mei: formal analysis. Zhaochi Feng: conceptualization, supervision. Jihong Yu: conceptualization, project administration, supervision, writing-review & editing, funding acquisition.

Conflicts of interest

There is no conflict of interest to report.

Acknowledgements

We thank the National Key Research and Development Program of China (Grant No. 2022YFA150360), the National Natural Science Foundation of China (Grant No. 22288101), and the '111 Center' (B17020) for supporting this work. We thank beamline BL14W1 of the Shanghai Synchrotron Radiation Facility for providing the beam time.

Notes and references

1 A. Corma, *Chem. Rev.*, 1997, **97**, 2373–2419.
2 W. J. Roth, P. Nachtigall, R. E. Morris and J. Čejka, *Chem. Rev.*, 2014, **114**, 4807–4837.
3 M. Shamzhy, M. Opanasenko, P. Concepción and A. Martínez, *Chem. Soc. Rev.*, 2019, **48**, 1095–1149.
4 H. Zhou, X. Yi, Y. Hui, L. Wang, W. Chen, Y. Qin, M. Wang, J. Ma, X. Chu, Y. Wang, X. Hong, Z. Chen, X. Meng, H. Wang, Q. Zhu, L. Song, A. Zheng and F.-S. Xiao, *Science*, 2021, **372**, 76–80.
5 Q. Zhang, S. Gao and J. Yu, *Chem. Rev.*, 2022, **123**, 6039–6106.
6 Y. Bai, D. Hao, Y. Wei, J. Han, D. Li, M. Chen and J. Yu, *Mater. Chem. Front.*, 2024, **8**, 2142–2148.
7 D. T. Bregante, M. C. Chan, J. Z. Tan, E. Z. Ayla, C. P. Nicholas, D. Shukla and D. W. Flaherty, *Nat. Catal.*, 2021, **4**, 797–808.

8 X. Yu, K. Liu, H. Zhang, B. Wang, G. Yang, J. Li and J. Yu, *CCS Chem.*, 2021, **3**, 252–264.
9 R. J. Lewis, K. Ueura, X. Liu, Y. Fukuta, T. E. Davies, D. J. Morgan, L. Chen, J. Qi, J. Singleton, J. K. Edwards, S. J. Freakley, C. J. Kiely, Y. Yamamoto and G. J. Hutchings, *Science*, 2022, **376**, 615–620.
10 P. Gao, S. Li, X. Bu, S. Dang, Z. Liu, H. Wang, L. Zhong, M. Qiu, C. Yang, J. Cai, W. Wei and Y. Sun, *Nat. Chem.*, 2017, **9**, 1019–1024.
11 Y. Wei, M. Chen, X. Ren, Q. Wang, J. Han, W. Wu, X. Yang, S. Wang and J. Yu, *CCS Chem.*, 2022, **4**, 1708–1719.
12 G. Perego, G. Bellussi, C. Corno, M. Taramasso, F. Buonomo and A. Esposito, *US pat.*, US 4 410 501, 1983.
13 O. Kwon, E. Zeynep Ayla, D. S. Potts and D. W. Flaherty, *Angew. Chem., Int. Ed.*, 2024, **63**, e202405950.
14 D. T. Bregante, A. M. Johnson, A. Y. Patel, E. Z. Ayla, M. J. Cordon, B. C. Bukowski, J. Greeley, R. Gounder and D. W. Flaherty, *J. Am. Chem. Soc.*, 2019, **141**, 7302–7319.
15 R. Bai, Y. Song, L. Lätsch, Y. Zou, Z. Feng, C. Copéret, A. Corma and J. Yu, *Chem. Sci.*, 2022, **13**, 10868–10877.
16 R. Bai, M. T. Navarro, Y. Song, T. Zhang, Y. Zou, Z. Feng, P. Zhang, A. Corma and J. Yu, *Chem. Sci.*, 2020, **11**, 12341–12349.
17 R. Bai, Y. Song, G. Tian, F. Wang, A. Corma and J. Yu, *Green Energy Environ.*, 2023, **8**, 163–172.
18 D. Zhou, T. Zhang, Q. Xia, Y. Zhao, K. Lv, X. Lu and R. Nie, *Chem. Sci.*, 2016, **7**, 4966–4972.
19 B. Notari, *Catal. Today*, 1993, **18**, 163–172.
20 P. T. Tanev, M. Chibwe and T. J. Pinnavaia, *Nature*, 1994, **368**, 321–323.
21 D. P. Serrano, R. Sanz, P. Pizarro, I. Moreno, P. de Frutos and S. Blázquez, *Catal. Today*, 2009, **143**, 151–157.
22 R. Bai, Y. Song, Y. Li and J. Yu, *Trends Chem.*, 2019, **1**, 601–611.
23 C. Wang, Y. Chu, Q. Lei, M. Hu, F. Deng, J. Xu and W. Dai, *Angew. Chem., Int. Ed.*, 2024, **63**, e202404633.
24 Q. Zhang, J. Li, G. He, J. Li, Z. Chen, Q. Zhang, C. Wang, G. Qi, Q. Wang, P. Zhang, J. Xu, O. Terasaki, D. Mei, Z. Liu and J. Yu, *CCS Chem.*, 2024, DOI: 10.31635/ccschem.024.202404123.
25 Y. Wang, H. Yang, Y. Zuo, D. Tian, G. Hou, Y. Su, Z. Feng, X. Guo and C. Li, *Appl. Catal., B*, 2023, **325**, 122396.
26 M. Signorile, L. Braglia, V. Crocellà, P. Torelli, E. Groppo, G. Ricchiardi, S. Bordiga and F. Bonino, *Angew. Chem., Int. Ed.*, 2020, **59**, 18145–18150.
27 S. Du, F. Li, Q. Sun, N. Wang, M. Jia and J. Yu, *Chem. Commun.*, 2016, **52**, 3368–3371.
28 W. Fan, R.-G. Duan, T. Yokoi, P. Wu, Y. Kubota and T. Tatsumi, *J. Am. Chem. Soc.*, 2008, **130**, 10150–10164.
29 Z. Liu and R. J. Davis, *J. Phys. Chem.*, 1994, **98**, 1253–1261.
30 R. Li, A. Smolyakova, G. Maayan and J. D. Rimer, *Chem. Mater.*, 2017, **29**, 9536–9546.
31 A. I. Lupulescu, W. Qin and J. D. Rimer, *Langmuir*, 2016, **32**, 11888–11898.
32 C. Sun, Z. Liu, S. Wang, H. Pang, R. Bai, Q. Wang, W. Chen, A. Zheng, W. Yan and J. Yu, *CCS Chem.*, 2021, **3**, 189–198.
33 Q. Guo, Z. Feng, G. Li, F. Fan and C. Li, *J. Phys. Chem. C*, 2013, **117**, 2844–2848.
34 J. Wang, Y. Zhao, T. Yokoi, J. N. Kondo and T. Tatsumi, *ChemCatChem*, 2014, **6**, 2719–2726.
35 J. Zhang, H. Shi, Y. Song, W. Xu, X. Meng and J. Li, *Inorg. Chem. Front.*, 2021, **8**, 3077–3084.
36 A. Jawor, B.-H. Jeong and E. M. V. Hoek, *J. Nanopart. Res.*, 2009, **11**, 1795–1803.
37 Y. Wang, L. Li, R. Bai, S. Gao, Z. Feng, Q. Zhang and J. Yu, *Chin. J. Catal.*, 2021, **42**, 2189–2196.
38 J. Zhang, R. Bai, Y. Zhou, Z. Chen, P. Zhang, J. Li and J. Yu, *Chem. Sci.*, 2022, **13**, 13006–13014.
39 G. Xiong, Y. Cao, Z. Guo, Q. Jia, F. Tian and L. Liu, *Phys. Chem. Chem. Phys.*, 2016, **18**, 190–196.
40 Y. Zuo, M. Liu, M. Ma, Y. Wang, X. Guo and C. Song, *ChemistrySelect*, 2016, **1**, 6160–6166.
41 Q. Guo, K. Sun, Z. Feng, G. Li, M. Guo, F. Fan and C. Li, *Chem. - Eur. J.*, 2012, **18**, 13854–13860.